

1 **High-order cognition is supported by complex but**
2 **compressible brain activity patterns**

3 Lucy L. W. Owen^{1,2} and Jeremy R. Manning^{1,*}

4 ¹Department of Psychological and Brain Sciences,
5 Dartmouth College, Hanover, NH

6 ²Carney Institute for Brain Sciences,
7 Brown University, Providence, RI

8 *Address correspondence to jeremy.r.manning@dartmouth.edu

9 February 27, 2023

10 **Abstract**

11 We applied dimensionality reduction algorithms and pattern classifiers to functional neu-
12 roimaging data collected as participants listened to a story, temporally scrambled versions of
13 the story, or underwent a resting state scanning session. These experimental conditions were
14 intended to require different depths of processing and inspire different levels of cognitive en-
15 gagement. We considered two primary aspects of the data. First, we treated the number of
16 features (components) required to achieve a threshold decoding accuracy as a proxy for the
17 “compressibility” of the neural patterns (where fewer components indicate greater compres-
18 sion). Second, we treated the maximum achievable decoding accuracy across participants as
19 an indicator of the “stability” of the recorded patterns. Overall, we found that neural patterns
20 recorded as participants listened to the intact story required fewer features to achieve compa-
21 rable classification accuracy to the other experimental conditions. However, the peak decoding
22 accuracy (achievable with more features) was also highest during intact story listening. Taken
23 together, our work suggests that our brain networks flexibly reconfigure according to ongoing
24 task demands, and that the activity patterns associated with higher-order cognition and high
25 engagement are both more complex and more compressible than the activity patterns associated
26 with lower-order tasks and lower levels of engagement.

27 **Keywords:** information, compression, temporal decoding, dimensionality reduction, neu-
28 roimaging

29 **Introduction**

30 Large-scale networks, including the human brain, may be conceptualized as occupying one or
31 more positions along on a continuum. At one extreme, every node is fully independent of every
32 other node. At the other extreme, all nodes behave identically. Each extreme optimizes key
33 properties of how the network functions. When every node is independent, the network is

29 maximally *expressive*: if we define the network’s “state” as the activity pattern across its nodes,
30 then every state is equally reachable by a network with fully independent nodes. On the other
31 hand, a network of identically behaved nodes optimizes *robustness*: any subset of nodes may
32 be removed from the network without any loss of function or expressive power, as long as any
33 single node remains. Presumably, most natural systems tend to occupy positions between these
34 extremes. We wondered: might the human brain reconfigure itself to be more flexible or more
35 robust according to ongoing demands? In other words, might the brain reconfigure its connections
36 or behaviors under different circumstances to change its position along this continuum?

37 Closely related to the above notions of expressiveness versus robustness are measures of
38 how much *information* is contained in a given signal or pattern, and how *redundant* a signal
39 is (Shannon, 1948). Formally, information is defined as the amount of uncertainty about a given
40 variables’ outcomes (i.e., entropy), measured in *bits*, or the optimal number of yes/no questions
41 needed to reduce uncertainty about the variable’s outcomes to zero. Highly complex systems with
42 many degrees of freedom (i.e., high flexibility and expressiveness), are more information-rich than
43 simpler or more constrained systems. The redundancy of a signal denotes the difference how
44 expressive the signal *could* be (i.e., proportional to the number of unique states or symbols used
45 to transmit the signal) and the actual information rate (i.e., the entropy of each individual state or
46 symbol). If a brain network’s nodes are fully independent, then the number of bits required to
47 express a single activity pattern is proportional to the number of nodes. The network would also
48 be minimally redundant, since the status of every node would be needed to fully express a single
49 brain activity pattern. If a brain network’s nodes are fully coupled and identical, then the number
50 of bits required to express a single activity pattern is proportional to the number of unique states
51 or values any individual node can take on. Such a network would be highly redundant, since
52 knowing any individual node’s state would be sufficient to recover the full-brain activity pattern.
53 Highly redundant systems are also robust, since there is little information loss from losing any
54 given observation.

55 We take as a given that brain activity is highly flexible: our brains can exhibit nearly infinite ac-
56 tivity patterns. This flexibility implies that our brains activity patterns are highly information rich.
57 However, brain activity patterns are also highly structured. For example, full-brain correlation
58 matrices are stable within (Finn et al., 2015, 2017; Gratton et al., 2018) and across (Yeo et al., 2011;

59 Glerean et al., 2012; Gratton et al., 2018; Cole et al., 2014) individuals. This stability suggests that
60 our brains' activity patterns are at least partially constrained, for example by anatomical, external,
61 or internal factors. Constraints on brain activity that limit its flexibility decrease expressiveness
62 (i.e., its information rate). However, constraints on brain activity also increase its robustness to
63 noise (e.g., “missing” or corrupted signals may be partially recovered). For example, recent work
64 has shown that full-brain activity patterns may be reliably recovered from only a relatively small
65 number of implanted electrodes (Owen et al., 2020; Scangos et al., 2021). This robustness property
66 suggests that the relevant signal (e.g., underlying factors that have some influence over brain
67 activity patterns) are compressible.

68 To the extent that brain activity patterns contain rich task-relevant information, we should
69 be able to use the activity patterns to accurately differentiate between different aspects of the
70 task (e.g., using pattern classifiers; Norman et al., 2006). For example, prior work has shown a direct
71 correspondence between classification accuracy and the information content of a signal (Alvarez,
72 2002). To the extent that brain activity patterns are compressible, we should be able to generate
73 simplified (e.g., lower dimensional) representations of the data while still preserving the relevant
74 or important aspects of the original signal. In general, information content and compressibility are
75 related but are partially dissociable (Fig. 1). If a given signal (e.g., a representation of brain activity
76 patterns) contains more information about ongoing cognitive processes, then the peak decoding
77 accuracy should be high. And if the signal is compressible, a low-dimensional embedding of the
78 signal will be similarly informative to the original signal (Fig. 1D).

79 Several recent studies suggest that the complexity of brain activity is task-dependent, whereby
80 simpler tasks with lower cognitive demands are reflected by simpler and more compressible brain
81 activity patterns, and more complex tasks with higher cognitive demands are reflected by more
82 complex and less compressible brain activity patterns (Mack et al., 2020; Owen et al., 2021). These
83 findings complement other work suggesting that functional connectivity (correlation) patterns are
84 task-dependent (Finn et al., 2017; Owen et al., 2020; Cole et al., 2014), although see Gratton et
85 al. (2018). Higher-order cognitive processing of a common stimulus also appears to drive more
86 stereotyped task-related activity and functional connectivity across individuals (Hasson et al.,
87 2008; Lerner et al., 2011; Simony & Chang, 2020; Simony et al., 2016).

88 The above studies are consistent with two potential descriptions of how cognitive processes are

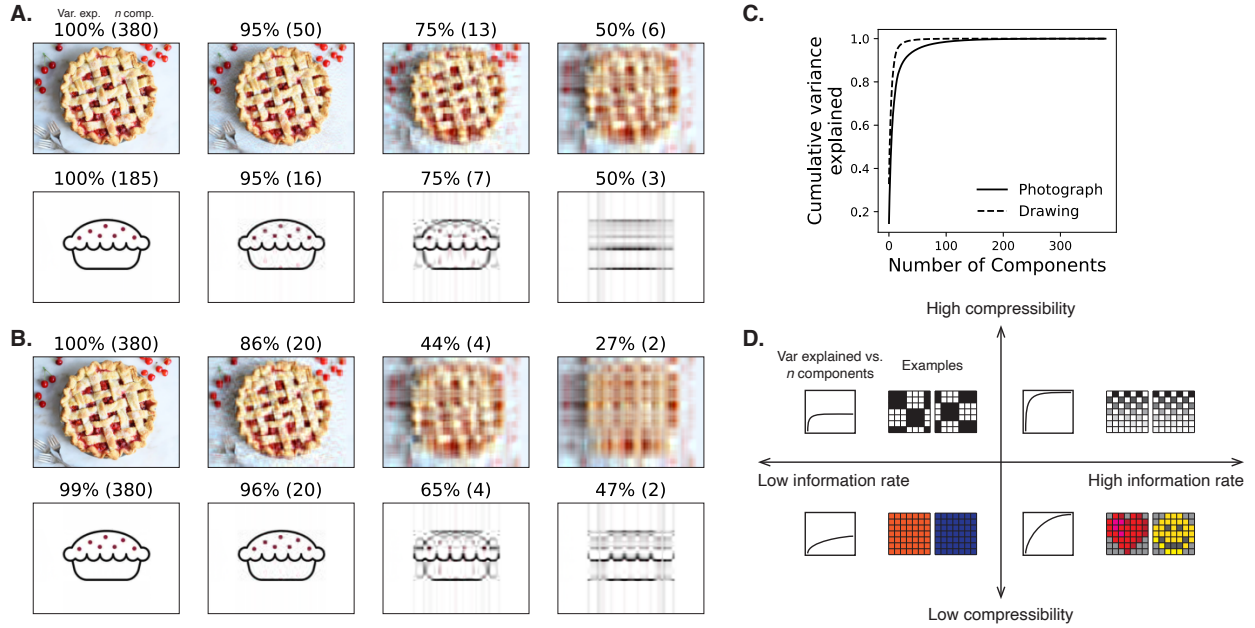


Figure 1: Information content and compressibility. **A. Variance explained for two images.** We applied principal components analysis to a photograph and drawing, treating each row of the images as “observations.” Across columns, we identified the number of components required to explain 100%, 95%, 75%, or 50% of the cumulative variance in each image (the 100% columns denote the original images). The numbers of components are indicated in parentheses, and the resulting “compressed” images are displayed. **B. Representing two images with different numbers of components.** Using the same principal component decompositions as in Panel A, we computed the cumulative proportion of variance explained with 380 (original images), 20, 4, or 2 components. **C. Cumulative variance explained versus number of components.** For the images displayed in Panels A and B, we plot the cumulative proportion of variance explained as a function of the number of components used to represent each image. **D. Information rate and compressibility.** Across multiple images, the information rate (i.e., the amount of information contained in each image; horizontal axis) is high when each individual pixel provides information that cannot be inferred from other pixels. High-information rate images tend to be high-resolution, and low-information rate images tend to be low-resolution. Compressibility is related to the difference between the information required to specify the original versus compressed images (vertical axis). Highly compressible images often contain predictable structure (redundancies) that can be leveraged to represent the images much more efficiently than in their original feature spaces.

89 reflects in brain activity patterns. One possibility is that the information rate of brain activity in-
90 creases during more complex or higher-level cognitive processing. If so, then the ability to reliably
91 decode cognitive states from brain activity patterns should improve with task complexity or with
92 the level (or “depth”) of cognitive processing. A second possibility is that the compressibility of
93 brain activity patterns increases during more complex or higher-level cognitive processing. If so,
94 then individual features of brain recordings, or compressed representations of brain recordings,
95 should carry more information during complex or high-level (versus simple or low-level) cognitive
96 tasks.

97 We used a previously collected neuroimaging dataset to estimate the extent to which each of
98 these two possibilities might hold. The dataset we examined comprised functional magnetic reso-
99 nance imaging (fMRI) data collected as participants listened to an audio recording of a 10-minute
100 story, temporally scrambled recordings of the story, or underwent a resting state scan (Simony
101 et al., 2016). Each of these experimental conditions evokes different depths of cognitive process-
102 ing (Simony et al., 2016; Lerner et al., 2011; Hasson et al., 2008; Owen et al., 2021). We used
103 across-participant classifiers to decode listening times in each condition, as a proxy for how “in-
104 formative” the task-specific activity patterns were (Simony & Chang, 2020). We also use principle
105 components analysis to generate lower-dimensional representations of the activity patterns. We
106 then repeated the classification analyses after preserving different numbers of components and
107 examined how classification accuracy changed across the different experimental conditions.

108 Results

109 We sought to understand whether higher-level cognition is reflected by more reliable and in-
110 formative brain activity patterns, and how compressibility of brain activity patterns relates to
111 cognitive complexity. We developed a computational framework for systematically assessing the
112 informativeness and compressibility of brain activity patterns recorded under different cognitive
113 circumstances. We used across-participant decoding accuracy (see *Forward inference and decoding*
114 *accuracy*) as a proxy for informativeness. To estimate the compressibility of the brain patterns, we
115 used group principal components analysis (PCA) to project the brain patterns into k -dimensional
116 spaces, for different values of k (see *Hierarchical Topographic Factor Analysis (HTFA)* and *Principal*

117 components analysis (PCA)). For more compressible brain patterns, decoding accuracy should be
118 more robust to small values of k .

119 We analyzed a dataset collected by Simony et al. (2016) that comprised four experimental
120 conditions. These conditions exposed participants to stimuli that systematically varied in cognitive
121 engagement. In the *intact* experimental condition, participants listened to an audio recording of
122 a 10-minute story. In the *paragraph*-scrambled experimental condition, participants listened to a
123 temporally scrambled version of the story, where the paragraphs occurred out of order, but where
124 the same set of paragraphs was presented over the entire listening interval. All participants in
125 this condition experienced the scrambled paragraphs in the same order. In the *word*-scrambled
126 experimental condition, participants listened to a temporally scrambled version of the story, where
127 the words occurred in a random order. Again, all participants in this condition experienced the
128 scrambled words in the same order. Finally, in the *rest* experimental condition, participants lay
129 in the scanner with no overt stimulus, while keeping their eyes open and blinking as needed.
130 This public dataset provided a convenient means for testing our hypothesis that different levels
131 of cognitive processing and engagement affect how informative and compressible the associated
132 brain patterns are.

133 Discussion

134 Methods

135 We measured properties of recorded neuroimaging data under different task conditions that varied
136 systematically in cognitive engagement and depth of processing. We were especially interested in
137 how *informative* and *compressible* the activity patterns were under these different conditions (Fig. 1).

138 Functional neuroimaging data collected during story listening

139 We examined an fMRI dataset collected by Simony et al. (2016) that the authors have made publicly
140 available at arks.princeton.edu/ark:/88435/dsp015d86p269k. The dataset comprises neuroimaging
141 data collected as participants listened to an audio recording of a story (intact condition; 36 par-
142 ticipants), listened to temporally scrambled recordings of the same story (17 participants in the

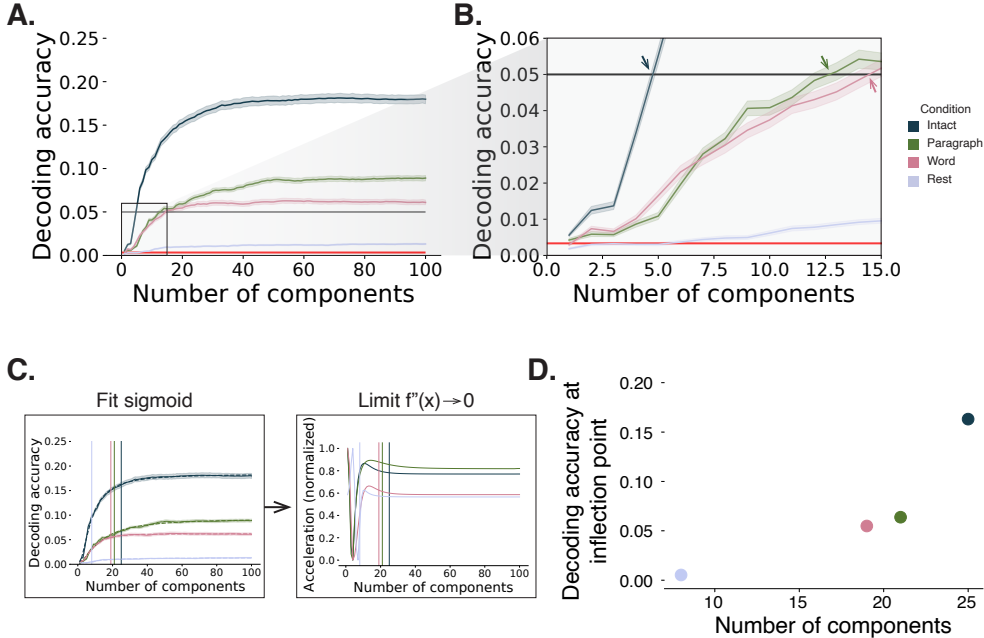


Figure 2: Decoding accuracy and compression. **A. Decoding accuracy by number of components.** Ribbons of each color display cross-validated decoding performance for each condition (intact, paragraph, word, and rest), as a function of the number of components (features) used to represent the data. The horizontal red line denotes chance performance, and the horizontal black line denotes 5% decoding accuracy (used as a reference in Panel B). **B. Numbers of components required to reach a fixed decoding accuracy threshold, by condition.** The panel displays a zoomed-in view of the inset in Panel A. Intersections between each condition’s decoding accuracy curve and the 5% decoding accuracy reference line are marked by arrows. **C. Estimating inflection points.** We sought to identify an “inflection point” for each decoding curve, denoting the number of components at which the decoding curve asymptotes. We fit sigmoid functions to each decoding curve (left sub-panel) and then computed the minimum number of components where the second derivative of the sigmoid was both positive and less than a threshold value of 0.0001. **D. Inflection points by condition.** Each dot displays the number of components (x -axis) and decoding accuracy (y -axis) at one condition’s inflection point. All error ribbons denote bootstrap-estimated 95% confidence intervals.

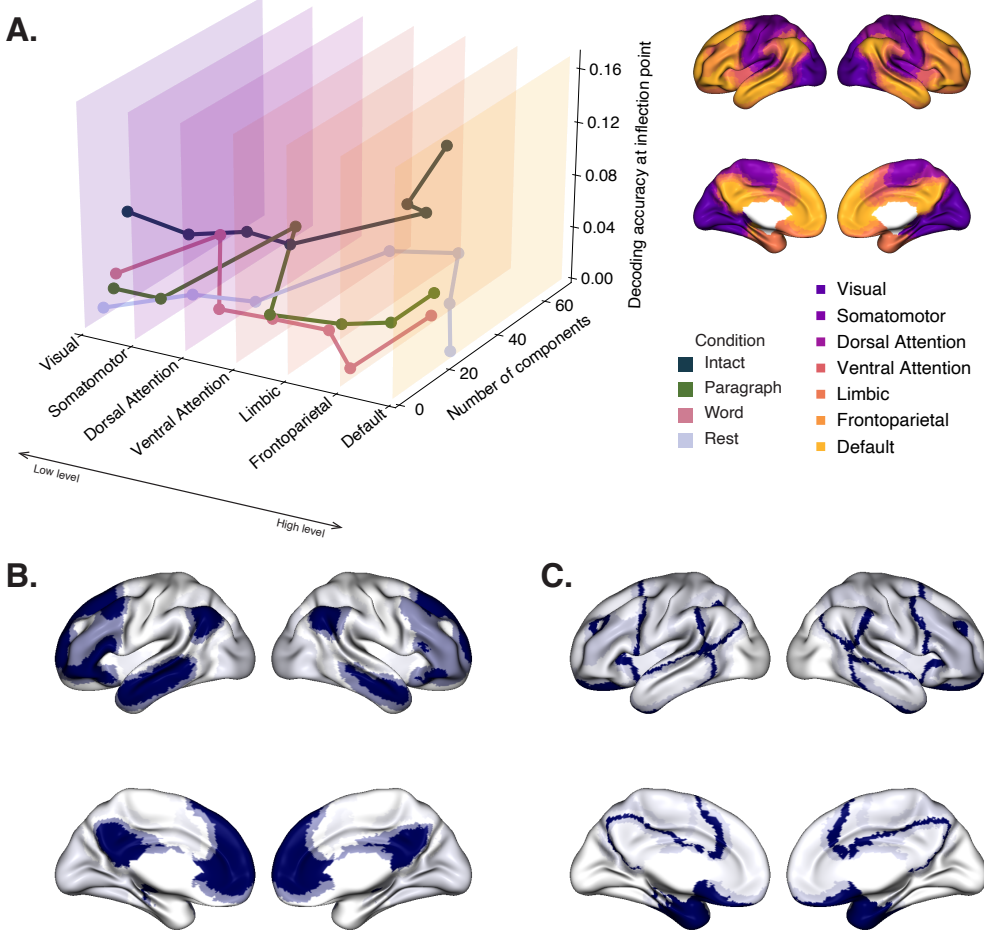


Figure 3: Network-specific decoding accuracy and compression. A. Decoding accuracy and number of components for network-specific inflection points. We considered the seven networks identified by Yeo et al. (2011). We computed each network's inflection point, for each experimental condition, using the procedure described in Figure 2C. **B. Network-specific decoding accuracy.** Each of the seven networks are colored according to the decoding accuracy at the network's inflection point for the "intact" experimental condition (corresponding to the dark blue curve in Panel A). **C. Network-specific compression.** Each of the seven networks are colored according to the number of components at the network's inflection point for the intact experimental condition. Larger numbers of components reflect lower compressibility.

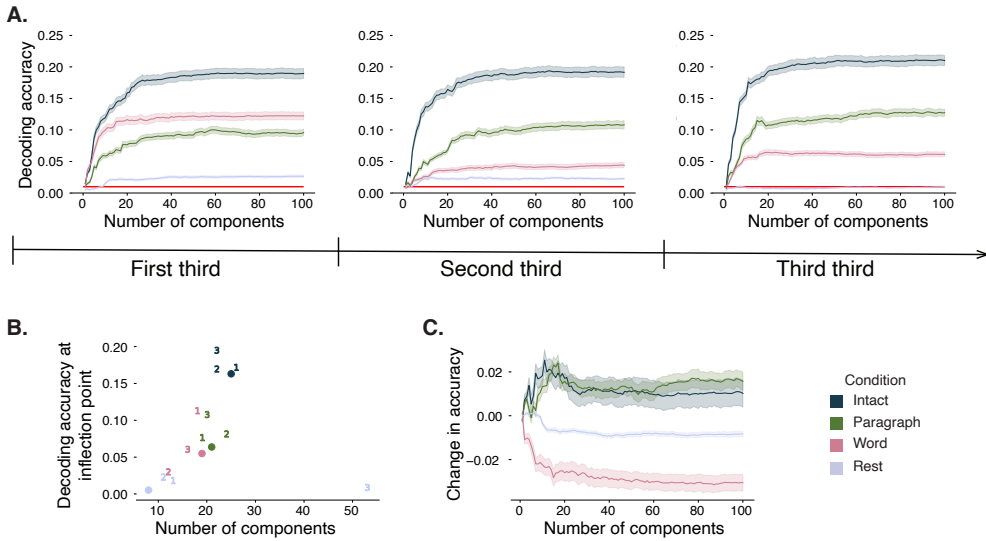


Figure 4: Changes in decoding accuracy and compression over time. **A. Decoding accuracy by number of components, by story segment.** Each family of curves is plotted in the same format as Figure 2A but reflects data only from one third of the dataset. **B. Inflection points by condition and segment.** The dots re-plot the inflection points from Figure 2D for reference. The numbers denote the inflection points for each third of the dataset (1: first third; 2: second third; 3: third third; colors denote experimental conditions). **C. Change in decoding accuracy over time, by number of components.** For each number of components (x-axis) and condition (color), we fit a regression line to the decoding accuracies obtained for the first, second, and third thirds of the dataset (corresponding to the left, middle, and right columns of Panel A, respectively). The y-axis denotes the slopes of the regression lines. All error ribbons denote bootstrap-estimated 95% confidence intervals.

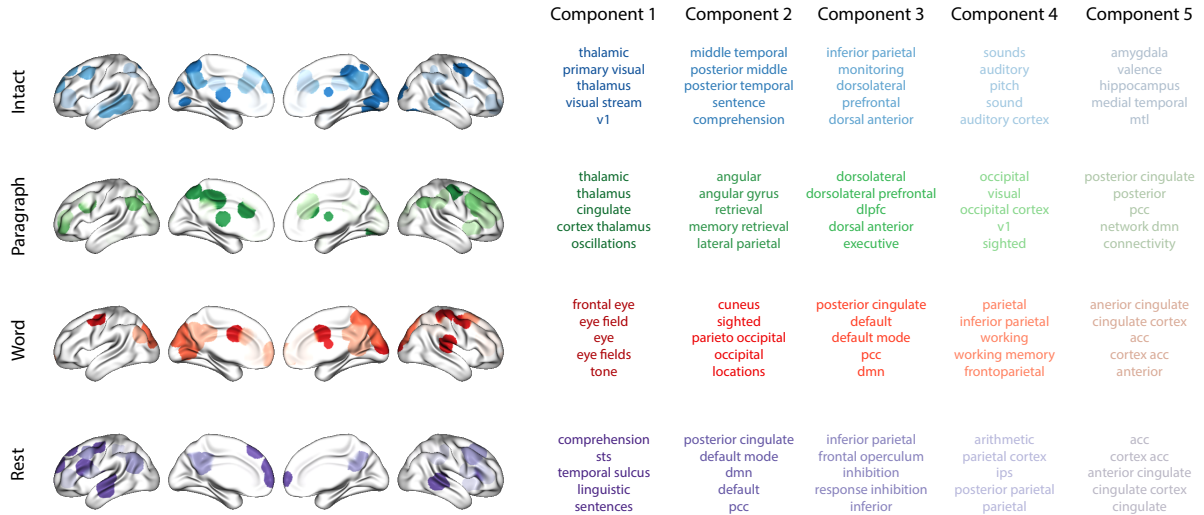


Figure 5: Top terms associated with the highest-weighted components by condition. Each row corresponds to an experimental condition, and the colors correspond to the component number (ranked by proportion of variance explained). The inflated brain plots display the top 20 highest-weighted hubs (see *Topographic Factor Analysis*) for each components'. The lists on the right display the top five Neurosynth terms (Rubin et al., 2017) decoded from each components' brain map. Analogous maps computed separately for each story segment may be found in Figure S1.

143 paragraph-scrambled condition listened to the paragraphs in a randomized order and 36 in the
 144 word-scrambled condition listened to the words in a randomized order), or lay resting with their
 145 eyes open in the scanner (rest condition; 36 participants). Full neuroimaging details may be found
 146 in the original paper for which the data were collected Simony et al. (2016). Procedures were
 147 approved by the Princeton University Committee on Activities Involving Human Subjects, and by
 148 the Western Institutional Review Board (Puyallup, WA). All subjects were native English speakers
 149 with normal hearing and provided written informed consent.

150 Hierarchical topographic factor analysis (HTFA)

151 Following our prior related work, we used HTFA Manning et al. (2018) to derive a compact
 152 representation of the neuroimaging data. In brief, this approach approximates the timeseries
 153 of voxel activations (44,415 voxels) using a much smaller number of radial basis function (RBF)
 154 nodes (in this case, 700 nodes, as determined by an optimization procedure; Manning et al., 2018)).
 155 This provides a convenient representation for examining full-brain activity patterns and network
 156 dynamics. All of the analyses we carried out on the neuroimaging dataset were performed in this

157 lower-dimensional space. In other words, each participant's data matrix, \mathbf{X} , was a number-of-
158 timepoints (T) by 700 matrix of HTFA-derived factor weights (where the row and column labels
159 were matched across participants). Code for carrying out HTFA on fMRI data may be found as
160 part of the BrainIAK toolbox Capota et al. (2017); Kumar et al. (2021), which may be downloaded
161 at brainiak.org.

162 **Principal components analysis (PCA)**

163 We applied group PCA (Smith et al., 2014) separately to the HTFA-derived representations of the
164 data (i.e., factor loadings) from each experimental condition. Specifically, for each condition, we
165 considered the set of all participants' T by 700 factor weight matrices. We used group PCA to
166 project these 700-dimensional matrices into a series of k -dimensional spaces, for $k \in \{3, 4, 5, \dots, 700\}$.
167 This yielded a set of number-of-participants matrices, each with T rows and k columns.

168 **Temporal decoding**

169 We sought to identify neural patterns that reflected participants' ongoing cognitive processing of
170 incoming stimulus information. As reviewed by Simony et al. (2016), one way of homing in on
171 these stimulus-driven neural patterns is to compare activity patterns across individuals. In partic-
172 ular, neural patterns will be similar across individuals to the extent that the neural patterns under
173 consideration are stimulus-driven, and to the extent that the corresponding cognitive representa-
174 tions are reflected in similar spatial patterns across people Simony & Chang (2020). Following this
175 logic, we used an across-participant temporal decoding test developed by Manning et al. (2018) to
176 assess the degree to which different neural patterns reflected ongoing stimulus-driven cognitive
177 processing across people. The approach entails using a subset of the data to train a classifier to
178 decode stimulus timepoints (i.e., moments in the story participants listened to) from neural pat-
179 terns. We use decoding (forward inference) accuracy on held-out data, from held-out participants,
180 as a proxy for the extent to which the inputted neural patterns reflected stimulus-driven cognitive
181 processing in a similar way across individuals.

182 **Forward inference and decoding accuracy**

183 We used an across-participant correlation-based classifier to decode which stimulus timepoint
184 matched each timepoint's neural pattern. For a given value of k (i.e., number of principal com-
185 ponents), we first used group PCA to project the data from each condition into a k -dimensional
186 space. Next, we divided the participants into two groups: a template group, $\mathcal{G}_{\text{template}}$ (i.e., training
187 data), and a to-be-decoded group, $\mathcal{G}_{\text{decode}}$ (i.e., test data). We averaged the projected data within
188 each group to obtain a single T by k matrix for each group. Next, we correlated the rows of the two
189 averaged matrices to form a T by T decoding matrix, Λ . In this way, the rows of Λ reflected time-
190 points from the template group, while the columns reflected timepoints from the to-be-decoded
191 group. We used Λ to assign temporal labels to each timepoint (row) from the test group's ma-
192 trix, using the row of the training group's matrix with which it was most highly correlated. We
193 repeated this decoding procedure, but using $\mathcal{G}_{\text{decode}}$ as the template group and $\mathcal{G}_{\text{template}}$ as the
194 to-be-decoded group. Given the true timepoint labels (for each group), we defined the decoding
195 accuracy as the average proportion of correctly decoded timepoints, across both groups (where
196 chance performance is $\frac{1}{T}$). In Figures 2 and 4 we report the decoding accuracy for each condition
197 and value of k , averaged across $n = 100$ cross validation folds.

198 **Reverse inference**

199 To help interpret the brain activity patterns we found within the contexts of other studies, we
200 created summary maps of each principal component, for each experimental condition, by summing
201 together the 20 HTFA-derived RBF nodes (see *Hierarchical Topographic Factor Analysis*) with the
202 highest absolute value weights for each of the top 5 components (Figs. 5, S1). We then carried
203 out a meta analysis using Neurosynth Rubin et al. (2017) to identify the 5 terms most commonly
204 associated with the given map.

205 **Data and code availability**

206 All of the code used to produce the figures and results in this manuscript, along with links to the
207 corresponding datasets, may be found at github.com/ContextLab/pca_paper.

²⁰⁸ **Acknowledgements**

²⁰⁹ We acknowledge discussions with Rick Betzel, Emily Finn, and Jim Haxby. Our work was sup-
²¹⁰ ported in part by NSF CAREER Award Number 2145172 to J.R.M. The content is solely the re-
²¹¹ sponsibility of the authors and does not necessarily represent the official views of our supporting
²¹² organizations. The funders had no role in study design, data collection and analysis, decision to
²¹³ publish, or preparation of the manuscript.

²¹⁴ **Author contributions**

²¹⁵ Conceptualization: J.R.M. and L.L.W.O. Methodology: J.R.M. and L.L.W.O. Implementation: L.L.W.O.
²¹⁶ Analysis: L.L.W.O. Writing, Reviewing, and Editing: J.R.M. and L.L.W.O. Supervision: J.R.M.

²¹⁷ **References**

- ²¹⁸ Alvarez, S. A. (2002). *An exact analytical relation among recall, precision, and classification accuracy in*
²¹⁹ *information retrieval* (Technical Report No. BCCS-02-01). Boston College.
- ²²⁰ Capota, M., Turek, J., Chen, P.-H., Zhu, X., Manning, J. R., Sundaram, N., ... Shin, Y. S. (2017).
²²¹ *Brain imaging analysis kit*.
- ²²² Cole, M. W., Bassett, D. S., Power, J. D., Braver, T. S., & Petersen, S. E. (2014). Intrinsic and
²²³ task-evoked network architectures of the human brain. *Neuron*, 83(1), 238–251.
- ²²⁴ Finn, E. S., Scheinost, D., Finn, D. M., Shen, X., Papademetris, X., & Constable, R. T. (2017).
²²⁵ Can brain state be manipulated to emphasize individual differences in functional connectivity.
²²⁶ *NeuroImage*, 160, 140–151.
- ²²⁷ Finn, E. S., Shen, X., Scheinost, D., Rosenberg, M. D., Huang, J., Chun, M. M., ... Constable, R. T.
²²⁸ (2015). Functional connectome fingerprinting: identifying individuals using patterns of brain
²²⁹ connectivity. *Nature Neuroscience*, 18, 1664–1671.

- 230 Glerean, E., Salmi, J., Lahnakoski, J. M., Jääskeläinen, I. P., & Sams, M. (2012). Functional magnetic
231 resonance imaging phase synchronization as a measure of dynamic functional connectivity.
232 *Brain Connectivity*, 2(2), 91–101.
- 233 Gratton, C., Laumann, T. O., Nielsen, A. N., Greene, D. J., Gordon, E. M., Gilmore, A. W., ...
234 Petersen, S. E. (2018). Functional brain networks are dominated by stable group and individual
235 factors, not cognitive or daily variation. *Neuron*, 98(2), 439–452.
- 236 Hasson, U., Yang, E., Vallines, I., Heeger, D. J., & Rubin, N. (2008). A hierarchy of temporal
237 receptive windows in human cortex. *The Journal of Neuroscience*, 28(10), 2539–2550.
- 238 Kumar, M., Anderson, M. J., Antony, J. W., Baldassano, C., Brooks, P. P., Cai, M. B., ... Norman,
239 K. A. (2021). BrainIAK: the brain image analysis kit. *Aperture*, In press.
- 240 Lerner, Y., Honey, C. J., Silbert, L. J., & Hasson, U. (2011). Topographic mapping of a hierarchy of
241 temporal receptive windows using a narrated story. *The Journal of Neuroscience*, 31(8), 2906–2915.
- 242 Mack, M. L., Preston, A. R., & Love, B. C. (2020). Ventromedial prefrontal cortex compressesion
243 during concept learning. *Nature Communications*, 11(46), doi.org/10.1038/s41467-019-13930-8.
- 244 Manning, J. R., Zhu, X., Willke, T. L., Ranganath, R., Stachenfeld, K., Hasson, U., ... Norman,
245 K. A. (2018). A probabilistic approach to discovering dynamic full-brain functional connectivity
246 patterns. *NeuroImage*, 180, 243–252.
- 247 Norman, K. A., Polyn, S. M., Detre, G. J., & Haxby, J. V. (2006). Beyond mind-reading: multi-voxel
248 pattern analysis of fMRI data. *Trends in Cognitive Sciences*, 10(9), 424–430.
- 249 Owen, L. L. W., Chang, T. H., & Manning, J. R. (2021). High-level cognition during story listening is
250 reflected in high-order dynamic correlations in neural activity patterns. *Nature Communications*,
251 12(5728), doi.org/10.1038/s41467-021-25876-x.
- 252 Owen, L. L. W., Muntianu, T. A., Heusser, A. C., Daly, P., Scangos, K. W., & Manning, J. R. (2020). A
253 Gaussian process model of human electrocorticographic data. *Cerebral Cortex*, 30(10), 5333–5345.

- 254 Rubin, T. N., Kyojo, O., Gorgolewski, K. J., Jones, M. N., Poldrack, R. A., & Yarkoni, T. (2017).
255 Decoding brain activity using a large-scale probabilistic functional-anatomical atlas of human
256 cognition. *PLoS Computational Biology*, 13(10), e1005649.
- 257 Scangos, K. W., Khambhati, A. N., Daly, P. M., Owen, L. L. W., Manning, J. R., Ambrose, J. B.,
258 ... Chang, E. F. (2021). Biomarkers of depression symptoms defined by direct intracranial
259 neurophysiology. *Frontiers in Human Neuroscience, In press*.
- 260 Shannon, C. E. (1948). A mathematical theory of communication. *Bell System Technical Journal*,
261 27(3), 379–423.
- 262 Simony, E., & Chang, C. (2020). Analysis of stimulus-induced brain dynamics during naturalistic
263 paradigms. *NeuroImage*, 216, 116461.
- 264 Simony, E., Honey, C. J., Chen, J., & Hasson, U. (2016). Dynamic reconfiguration of the default
265 mode network during narrative comprehension. *Nature Communications*, 7(12141), 1–13.
- 266 Smith, S. M., Hyvärinen, A., Varoquaux, G., Miller, K. L., & Beckmann, C. F. (2014). Group-PCA
267 for very large fMRI datasets. *NeuroImage*, 101, 738–749.
- 268 Yeo, B. T. T., Krienen, F. M., Sepulcre, J., Sabuncu, M. R., Lashkari, D., Hollinshead, M., ... Buckner,
269 R. L. (2011). The organization of the human cerebral cortex estimated by intrinsic functional
270 connectivity. *Journal of Neurophysiology*, 106(3), 1125–1165.